Summary of the Ph.D. thesis presented by G. Grasselli on 27 June 2001 at the EPF-Lausanne, Switzerland.

Shear Strength of Rock Joints based on Quantified Surface Description

Ph.D. Thesis n.2404 (2001)

Presented by

G. Grasselli

At the Civil Engineering Department, EPF Lausanne, Switzerland

Present address: Department of Civil Engineering, University of Toronto, Toronto, ON, M5S 1K4, Canada
Tel. +1 416-978-0125, E-mail address: Giovanni.Grasselli@utoronto.ca Webpage: www.geogroup.utoronto.ca

Abstract

One of the primary objectives of this work is to improve the understanding of the frictional behaviour of rough rock joints under shear loads, and to relate its shear strength to the "shape" of the joint interface (roughness). Discontinuities have, indeed, an important influence on the deformational behaviour of rock systems. The choice of a general criterion to determine the shear strength of rough rock joints is a problem that has been investigated for many years. Numerous shear models have been proposed to relate shear-strength to measurable joint parameters, but their limitations have to be recognized. The main problem is how to measure and quantify the roughness in order to introduce the morphological aspect of the joint into a shear strength criterion. The first part of this work focuses on the measurement and description of how the roughness influences the size and distribution of contact areas during shearing. It has been found that the variation of the contact area can be express as function of the local dip inclination of the surface, measured along the shear direction. The close agreement between this empirical description of the potential contact area, and surface measurements permits to predict the real contact area involved in the phenomena. In the second part of the work, a new constitutive criterion, relating stress and displacements, is proposed to model the shear resistance of joints under constant normal load conditions. It is based on the proposed empirical roughness estimation, and on the results from more than fifty constant-normal-load direct-shear tests performed on replicas of tensile joints and on induced tensile fractures for seven rock types. This constitutive model is able to describe experimental shear tests conducted in the laboratory. Moreover, the parameters required in the model can be easily measured through standard laboratory tests. The proposed criterion was also used to estimate the JRC value. The predicting values were successfully correlated with JRC values obtained by back-analysis of shear tests.

1. Introduction

The determination of a general criterion to estimate the shear strength of rough rock joints is a problem that has been investigated for many years. Several criteria have been proposed in the past to identify the strength of a rough rock joint. These criteria delineate the state of stress that separates pre-sliding and post-sliding of the joint. Notable among them are Patton's model [1], Ladanyi's empirical model [2], Barton's empirical model [3], Amadei-Saeb's analytical model [4,5], Plesha's theoretical model [6]. All of them are two-dimensional models. While these models have improved our understanding of rock-joint behavior, their limitations have to be recognized. Moreover, it is necessary to stress the fact that among all the models proposed in the literature, Barton's criterion is the only one that is currently used in practice [7]. The method is based on choosing a value for the morphological parameter: the joint roughness coefficient (JRC). Several approaches, such as fractal analysis [8-13] or statistics [14], have been proposed to estimate the proper JRC value for a surface [15,16]. However, none of these methods are capable of always predicting the value of JRC that one would need to use in order to obtain the peak shear strength value measured during the shear test. Even though all these

approaches are useful for describing profiles, they are not sufficient to capture the features necessary for characterising three-dimensional roughness [17], and they have led to controversial findings [9,13,18]. In addition, roughness of natural rock joint planes is anisotropic, but anisotropic roughness quantification has not been clearly addressed in the literature [19-23]. Only recently have researchers focused their attention on identifying three-dimensional parameters to quantify the relationship between the surface roughness and shear strength [24-27]. Therefore, one current research topic is the three-dimensional characterisation of the roughness and its relationship with both initial contact area and stress distribution [28,29].

Today, technological advancements are making it increasingly possible to measure and characterize surfaces in three dimensions. Therefore, the challenge today is finding ways to quantify three-dimensional surface characteristics and incorporating new parameters into expressions of shear strength. To accomplish this requires not only the ability to measure and characterize surface roughness, but also the ability to express roughness as a number (e.g., JRC) or a mathematical expression. To be useful, these expressions must provide accurate estimates of peak-shear strength, based on parameters easily measured under both laboratory and *in-situ* conditions.

2. Measurement system

Measurement of roughness and contacts between two surfaces is a very challenging problem common to many different disciplines. Depending on the size we are investigating, researchers discriminate the different features of the surface in term of the form, waviness and roughness [30]. The roughness itself can be divided into macro-, micro- and submicro-roughness. The fact that the surface shape is scale-dependent leads to the conclusion that, depending on the problem, the scale at which we should resolve the surface morphology is different. For example, it is accepted that for studying the wear of very smooth surfaces (i.e. magnetic hard disks) it is necessary to measure the surface at nanometric resolution [31]. In rock mechanics, laboratory direct shear tests show that the size of the asperities that are damaged is on the order of millimetres, therefore a precision of $1/100^{th}$ of millimetre seems to be sufficient for a correct laboratory characterization of the rock joint. The facts lead us to conclude that the choice of the scale at which characterise the surface, as well as the proper measurement system to use, is linked to and dependent on the problem studied. One must indeed use not only the appropriate measuring device, but also one that is capable of resolving the least significant magnitude of the quantity desired, and which has sufficient range to cover the largest expected value. Using Kelvin's words, being able to describe and to quantify attributes allows us to move beyond "meagre" knowledge.

In this work, after an extended evaluation, a special optical measurement system, the ATS scanner [32], was adopted to digitise the entire rock joint surfaces (3D measurement). Such a system offers both the advantages of high precision and good repeatability, as well as being fast and easy to use [26]. Moreover, the weight and the dimensions of the transport cases make possible its utilization *in-situ*, assuring the same accuracy as in laboratory measurements [26].

The ATS topometric system works on a new principle compared to one-camera fringe projection sensors. During the measurement, various white-light fringe patterns are projected onto the object surface and recorded by two digital cameras, which are integrated into the measurement head, from two different angles (Figure 1). Three-dimensional coordinates are computed independently with high accuracy for each of the CCD camera pixels using triangulation methods and digital image processing (fringe projection and image shifting). The consistent exploitation of redun-

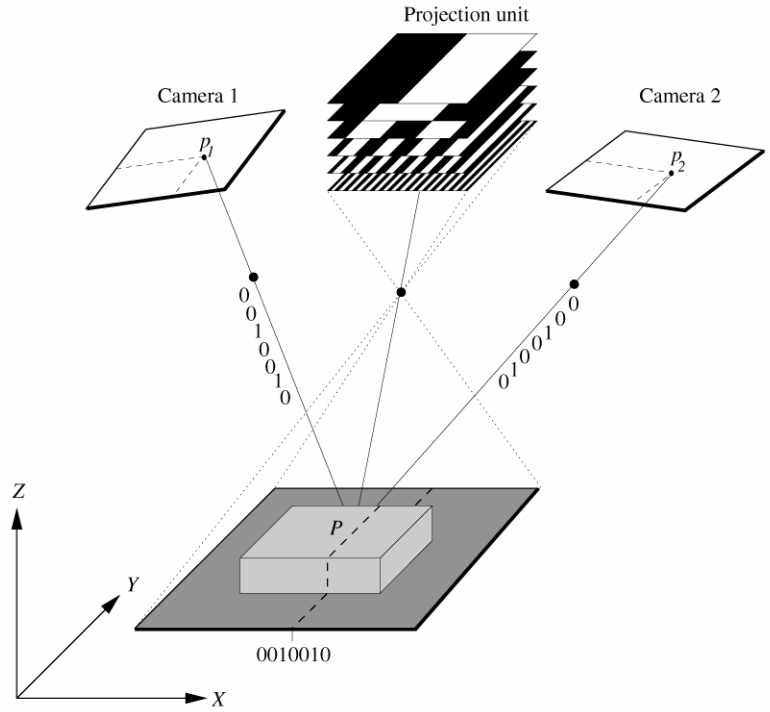

Figure 1. Principle of the advanced topometric sensor system [32].

dant information minimises the measurement errors. Due to the high data density resulting from the optical measurement process, details of the rough surface can be depicted precisely as point data. The accuracy of the point cloud has been computed to be ±50 μm for the measurement set-up chosen. It is comparable to that of accurate contact measuring machines and single range camera systems [24].

For the current research, the joint surfaces were reconstructed from the three-dimensional point clouds with a specially developed triangulation algorithm [33]. This approach results in a discretisation of the joint surface into contiguous triangles, defined by vertex and by the orientation of the vector normal to the plane of the triangle. The accuracy of the reconstruction depends on the density of measurements; the more dense the measurements, the higher the accuracy of the reconstruction. This method of discretisation of the joint surfaces is particularly advantageous for estimating the areas of the surfaces in contact during shearing.

3. Surface quantification

On sheared samples in the laboratory it was observed that the real contact area is only a small portion of the total area, and so is difficult to relate to a single profile. Moreover, the contact areas for the same rough surface (tests made on replicas) vary when changing shear direction and/or applied normal load (σ_n). As the shear strength of the joint, damage location, and joint morphology are strongly inter-dependent, it appears that only by studying the entire surface, and not just one profile, can it be possible to understand its influence on the shear strength.

The shape of the damage zones depends on the local geometry of the fracture surface, including the size and the shape of asperities, as well as on the mechanical parameters of the rock, and on the shear direction and the degree of stress and horizontal displacement [34]. As shear load is applied, the asperities dipping face to the shear direction start to deform elastically, and areas inclined opposite to the shear direction are detached, causing voids to appear perpendicular to the direction of shearing [35-37]. This behaviour is con-

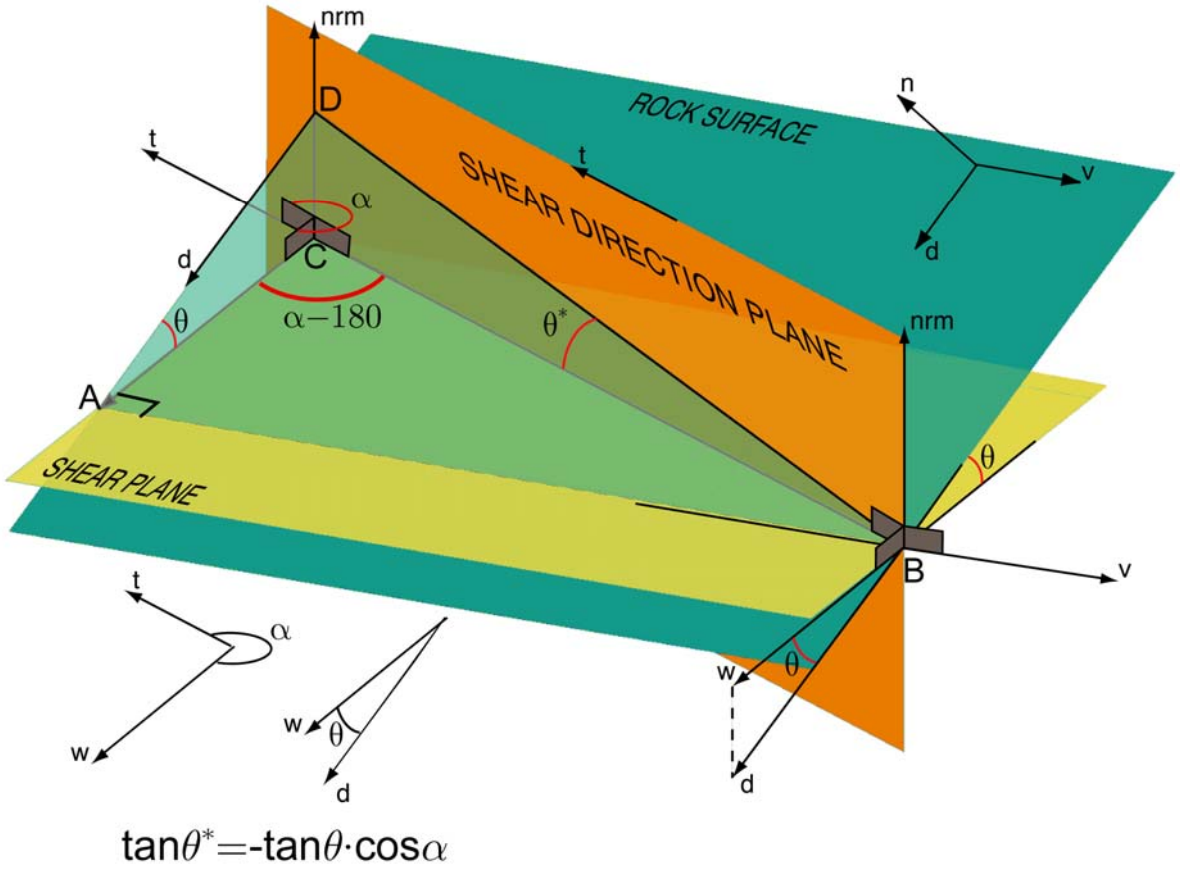

Figure 2. Geometrical identification of the apparent dip angle θ^*, in function of the shear direction.

sistent with the experimental results of fracture permeability obtained by Yeo et al. [38] and Gentier et al. [39]. Since the contact during shearing depends on the applied load, in order to localise the contact area on the reconstructed surface, it is first necessary to specify the shear direction.

It follows that on reconstructed surfaces, by triangulation, the contact could only occur on those triangles parallel to or facing the shear vector, but not on those opposite to it. Moreover, Yang and Chiang [36] have shown that the behaviour of a composite tooth-shaped joint with two different angled teeth is firstly dominated by the steeper tooth while the lower one participates only in the second part of shearing. For natural rock surfaces, laboratory observations make it possible to generalise this concept to say that, during the shearing, the stress is redistributed among different asperities, starting from the steepest. It follows that the identification of the potential damaged areas only requires the determination of the areas which face the shear direction and which, among them, are steep enough to be involved. The apparent dip angle describes the contribution of each triangle inclination (Figure 2). The visual comparison between the computed damaged area map, and the image of the joint surface after shearing shows that the prediction agrees well with the experimental observation (Figure 3) [26].

Based on the identification of the concept of threshold apparent dip angle, the shearing mechanism may be simplified by assuming that only those zones of the surface facing the shear direction, and steeper than a threshold apparent inclination (defined as θ^*_{cr}), unique for each applied normal load, are involved in the shearing. Among these zones, the areas of the surface inclined exactly at θ^*_{cr} will be just in contact, whereas the areas inclined more then θ^*_{cr} will be deformed, sheared or crushed, depending on the redistri-

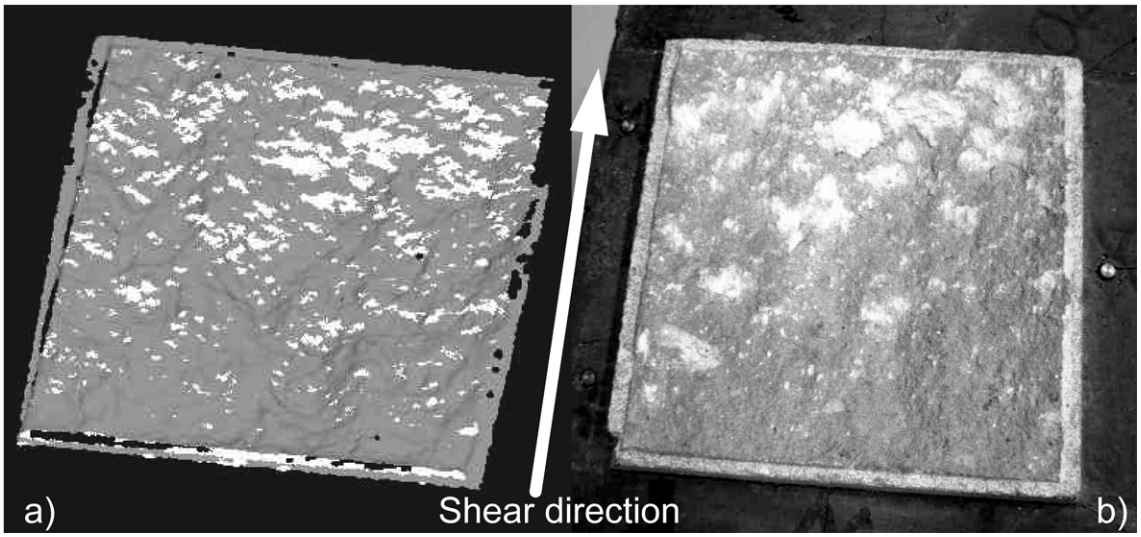

Figure 3. Identification of the areas damaged during the shear test.

bution of the normal load applied. In this way it is possible to discriminate the surface that might be damaged during shearing as a function of a threshold value θ^*_{cr}. The sum of all areas in contact or damaged during shearing is termed the "total potential contact area", A_{θ^*}; note that A_{θ^*} depends on the specified value of the threshold dip angle θ^*_{cr}, as well as on the normal load. To study the relationship between the potential contact area A_{θ^*} and the corresponding minimum apparent dip angle, the digitised surface data was used to calculate A_{θ^*} for several values of θ^*, and plotted on the A_{θ^*}-θ^* plane. The first approach in trying to quantify the relationship between A_{θ^*} and θ^* was to fit these points with an exponential function and a Gaussian function. Although these equations provide good fits to the data, they are unappealing in the sense that as A_{θ^*} ranges between 0 and A_0, θ^* ranges between 0 and infinity. The realistic upper bound on θ^* is equal to $\theta^*_{\max}$. To overcome this problem, the following equation was adopted to fit the data:

$$A_{\theta^*} = A_0 \left(\frac{\theta^*_{\max} - \theta^*}{\theta^*_{\max}} \right)^C \quad (1)$$

where A_0 is the maximum possible contact area in the shear direction, $\theta^*_{\max}$ is the maximum apparent dip angle in the shear direction, and C is a "roughness" parameter, calculated using a best-fit regression function, which characterises the distribution of the apparent dip angles over the surface [40]. The parameters A_0, C and $\theta^*_{\max}$ depend on the specified shear direction, as well as on the three-dimensional surface representation (i.e. triangulation algorithm and measurement resolution). Our laboratory tests showed that natural rock surfaces have $\theta^*_{\max}$ values in a range between 20 and 90 degrees. The parameter values obtained for all surfaces are reported in Table 1.

4. Evolution of surface parameters with shearing

Shearing causes two general types of damage: crushing and shearing of asperities. Mechanically, as the shear load is applied on the sample, the stress is redistributed, causing elastic deformations of the asperities up to failure. In the model this phenomenon progressively leads to more triangles being involved. Therefore, it is possible to state that shearing modifies the surface morphology.

Table 1. Comparison among results obtained fitting measurements with the proposed empirical description of the potential contact area. The expression is able to describe closely the surface (r^2 close to units), and moreover its parameters have an evident mechanical meaning.

Sample name	Rock type	A_0 [-]	C [-]	θ^*_{max} [deg]	θ^*_{max}/C [deg]	r^2 [-]
C1	Limestone	0.491	7.03	80	11.38	0.9988
C2	Limestone	0.462	5.64	80	14.19	0.9991
C3	Limestone	0.460	4.60	57	12.37	0.9977
C4	Limestone	0.508	4.74	65	13.72	0.9971
C5	Limestone	0.495	5.26	74	14.07	0.9989
C6	Limestone	0.546	5.19	68	13.11	0.9984
C8	Limestone	0.555	5.71	74	12.97	0.9979
G1	Granite	0.493	7.17	90	12.49	0.9975
G2	Granite	0.498	5.60	80	14.31	0.9986
G4	Granite	0.498	5.48	65	11.80	0.9967
G5	Granite	0.460	5.33	57	10.69	0.9989
G6	Granite	0.477	7.39	84	11.36	0.9985
G7	Granite	0.470	7.15	81	11.33	0.9980
G9	Granite	0.508	5.85	75	12.81	0.9986
Gn3	Gneiss	0.492	8.11	65	8.01	0.9970
Gn6	Gneiss	0.522	4.91	63	12.87	0.9993
Gn9	Gneiss	0.488	8.12	63	7.76	0.9966
Gn10	Gneiss	0.500	8.18	70	8.56	0.9953
Gn11	Gneiss	0.432	10.28	74	7.20	0.9979
Gn12	Gneiss	0.506	11.12	85	7.64	0.9953
Gn13	Gneiss	0.503	9.17	74	8.07	0.9958
M1	Marble	0.513	9.64	76	7.89	0.9954
M2	Marble	0.492	5.60	39	6.91	0.9961
M3	Marble	0.471	10.50	65	6.21	0.9987
M4	Marble	0.513	8.12	61	7.54	0.9967
M5	Marble	0.533	8.92	59	6.61	0.9989
M6	Marble	0.450	10.18	68	6.68	0.9978
M7	Marble	0.502	13.33	86	6.44	0.9938
M8	Marble	0.459	10.52	72	6.84	0.9961
M9	Marble	0.494	10.36	59	5.70	0.9977
M10	Marble	0.515	10.79	67	6.21	0.9972
M11	Marble	0.533	9.89	68	6.88	0.9968
M12	Marble	0.429	7.28	55	7.55	0.9975
ML1	Sandstone	0.573	7.25	66	9.10	0.9977
ML2	Sandstone	0.481	5.66	55	9.73	0.9985
ML3	Sandstone	0.523	7.81	66	8.45	0.9977
S1	Serpentinite	0.504	4.80	79	16.38	0.9994
S2	Serpentinite	0.466	4.44	75	16.84	0.9989

In this research, to gain some understanding of how surface parameters change with shearing, surfaces for several samples were measured before and after shear tests. One would expect shearing of asperities to occur at peak shear stress, and at those asperities with the steepest inclinations in the direction of shearing. The proposed model captures this behaviour, and it results in a corresponding decrease in θ^*_{max} that represents the smoothing of the damaged asperities. The parameter C also decreases, more than θ^*_{max}, and reflects the smoothing-out of the distribution of angularity due to shear damages. More uni-

Table 2. Evolution with shearing for the parameters of the surface characteristic curve.

Sample name	σ_n [MPa]	σ_n/σ_c [-]	A_0 [-]	C [-]	θ^*_{max} [deg]	r^2 [-]	θ^*_{max}/C [deg]
C2 (fresh)	-	-	0.462	5.64	80	0.9991	14.19
C2 (after 1 shearing)	1.12	0.04	0.462	4.19	65	0.9994	15.51
G9 (fresh)	-	-	0.508	5.85	75	0.9986	12.81
G9 (after 1 shearing)	1.12	0.006	0.493	4.85	65	0.9985	13.40
M12 (fresh)	-	-	0.429	7.28	55	0.9975	7.55
M12 (after 1 shearing)	1.80	0.02	0.405	7.14	55	0.9970	7.71
ML2 (fresh)	-	-	0.481	5.66	55	0.9985	9.73
ML2 (after 1 shearing)	4.13	0.42	0.466	5.55	55	0.9987	9.91

form roughness corresponds to an increase in the ratio θ^*_{max}/C with shearing (Table 2). The parameter A_0, which is the maximum potential contact area for the shear direction, changed very little during shearing because, in our experimental set-up, the shear plane is parallel to the average plane of the joint.

5. Anisotropy in shear strength

The assumption that shear strength depends on the direction of the motion was experimentally verified by shearing replicas of the identical surfaces in different directions. One serpentinite joint was the fracture chosen to be cast and analysed because its characteristic surface with anisotropic sinusoidal pattern. In order to visualise the surface anisotropy, the parameters A_0, C and θ^*_{max} were calculated all around the average-plane of the joint in steps of 5 degrees, and the values of ratio θ^*_{max}/C, obtained for each direction, were plotted in polar diagram [41] (Figure 4).

Furthermore, tilt tests were conducted in four different directions to confirm the results obtained during shear tests. The comparison between shear strength values obtained during laboratory tests, and morphological parameters calculated from surface measurements, results in a strict correlation (

Table 3). The values of peak shear strength obtained while shearing the sample in direction 0˚ and 180˚ are similar, as well as are the calculated surface parameters in those directions. Sheared in the 90˚ direction, the joint provides much less strength and the

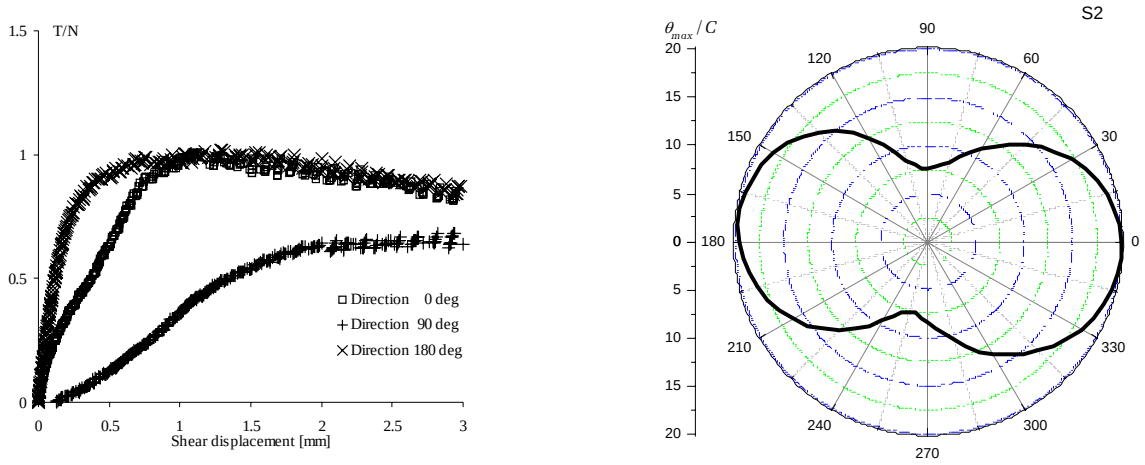

Figure 4. Replicas of the same serpentinite joint (S2) have been sheared in three different directions. The analysis of the surface roughness shows that along axis 0-180 the contribution is equal in both directions whereas is definitely lower in the perpendicular direction.

Table 3. Experimental results of shear strength and peak friction angle obtained by shearing replicas of the same joint (S2) along different directions: 0, 90, and 180 degrees. The anisotropic behaviour of the joint is illustrated by the morphological parameters, and the tilt tests.

Direction (deg)	Tilt Test (deg)	θ^*_{max}/C (deg)	T/N (-)	ϕ_{peak} (deg)
0	62	19.9	1.01	45
90	46	7.8	0.70	35
180	60	16.8	1.02	45
270	45	7.5	-	-

surface parameter results in a low value of θ^*_{max}/C. Therefore, it is possible to conclude that experimental results show the direction-dependency of the shear strength of rock joints, and demonstrate the ability of the proposed surface parameters to capture and quantify the effect of surface anisotropy on the shear strength of a fracture [40].

6. Influence of the applied normal stress on shearing of rough rock joints

In agreement with results obtained by other researchers [42,43], the effect of surface roughness on shear strength was found to be more pronounced for relatively low values of effective stress. By testing rough joints in replicas at extremely low values of normal stress ($\sigma_n/\sigma_c = 6 \times 10^{-4}$), it was found that shearing occurs by overriding the asperities, which remain unbroken. At higher values of normal stress ($\sigma_n/\sigma_c = 1.5 \times 10^{-2}$), the asperities begin to be sheared. The dilation is entirely replaced by shearing at a sufficiently high normal stress ($\sigma_n/\sigma_c = 0.15$~0.2). The experimental curves show that increasing the applied normal load (σ_n) the absolute value of peak shear strength (τ_p) increases (Figure 5). However, with increasing σ_n, the ratio τ_p/σ_n decreases (Figure 6). Beyond a critical normal load, which has been evaluated corresponding to $\sigma_n/\sigma_c = 0.2$ [42], τ_p/σ_n tends to a constant value (ultimate or residual shear resistance). This means that the role that surface morphology plays in shear resistance decreases with increasing normal load. When there is no applied normal load, the normal force acting on the joint is that resulting from the weight of the sample itself, and in this case the ratio of shear-to-normal load is maximum. The maximum peak-friction angle corresponds to this loading condition.

7. Shear tests on tensile rock joints

Generally, shearing of rock joints occurs *in-situ* under a variety of boundary conditions. However, it is possible to identify two different characteristic behaviours: the first condition, where the joint can freely dilate (e.g., rock slope), is duplicated in the laboratory by maintaining a constant normal load (CNL) under the shearing test; the second condition, where the joint is constrained and any dilation activates additional normal load (e.g., foundation piles or a block in a rock mass), is simulated in laboratory by keeping a constant normal stiffness (CNS) during the shearing. Nevertheless, the mechanical behaviour of shear tests made under CNL conditions or CNS conditions differs only after the peak, when dilation plays an important role, inducing an increment in the normal stress. Before reaching the peak, since almost no dilation has occurred, both types of shear test follow the same path [44-46]. Thus, for studying the joint behaviour up to the peak shear strength, it has been judged that the most appropriate laboratory experimental shear test set-up is the CNL. Therefore, more than fifty CNL direct-shear tests were performed in the laboratory on both replicas of tensile joints and induced tensile fractures, for seven rock types.

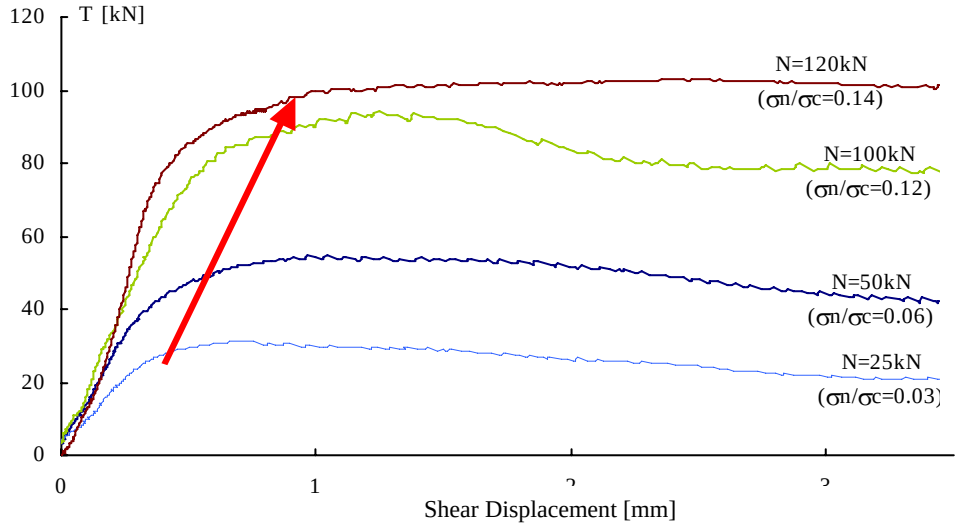

Figure 5. Several shear tests have been conducted on different samples with the same morphology (replicas of G2 granite joint). A sensible growth in shear resistance and a stiffer response of the joint follow the increasing of the applied normal load (in the sense of the arrow).

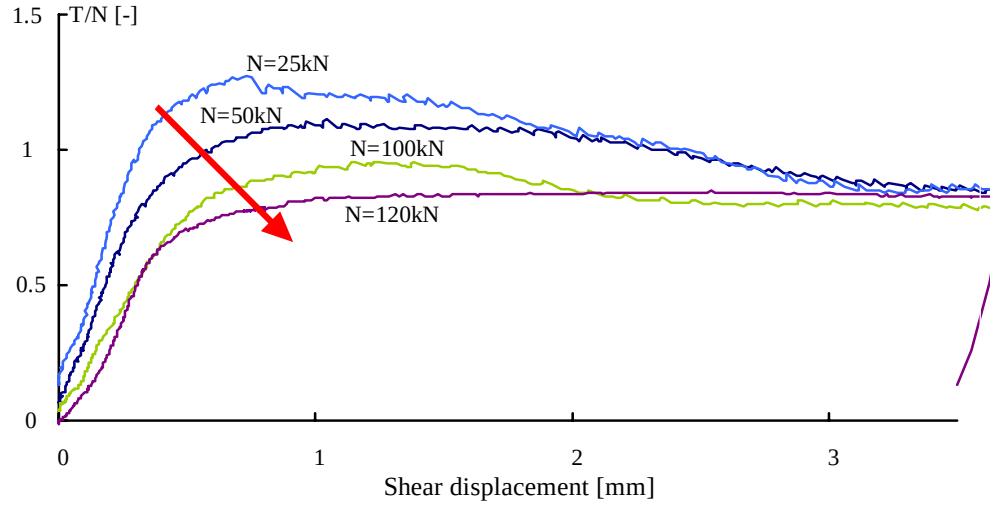

Figure 6. Plotting T/N vs. horizontal displacement for test results on replicas of G2 granite tensile joint, it is possible to remark that increasing of the applied normal load, the ratio T/N progressively decreases in the sense of the arrow, and, beyond a critical normal load (σ_n/σ_c=0.2) T/N tends to a constant value.

Concrete replicas of an induced joint in rock were first employed. The fact that replicas made from the same cast have identical surfaces permits one to perform several shear experiments on joints with the same morphology. The advantage of using replicas is that they allow the independent study of two parameters that most strongly influence shear behaviour: normal load and surface morphology. Using replicas of the same surface, morphological parameters are constant, thus allowing the investigation of the influence of normal load on peak shear strength. Moreover, by using replicas of the same surfaces and performing shear tests in different directions, the influence of the roughness-anisotropy on the frictional resistance could be examined. To validate and generalise this approach, casts were made of five different rock joints: one gneiss joint (Gn2), two granite joints (G8 and G2), and two serpentinite joints (S1 and S2).

The advantage of using rock-joint samples, rather than mortar replicas, is that they allow one to investi-

Table 4. Mechanical properties of rocks used in shear tests.

Material	Symbol	α	ρ	σ_c	σ_t	σ_c/σ_t	E	ϕ_b	ϕ_r	c_r
		[deg]	[t/m^3]	[MPa]	[MPa]	[-]	[GPa]	[deg]	[deg]	[MPa]
Gneiss	Gn	0	2.66	160	3.5	46	45.9	36	43	4.9
Gneiss	Gn	30	2.66	60	-	-	21.1	36	40	2.4
Gneiss	Gn	90	2.65	184	9.5	19	37.4	36	40	1.7
Tarn granite	G	-	2.70	173	8.8	20	48.4	34	51	0.8
Magny limestone	C	-	2.19	25	2.4	10	14.9	36	38	4.5
Pont du Gard limestone	CpG	-	1.94	5	1.0	5	3.6	37	32	1.3
Carrara marble	M	-	2.69	87	9.2	9	29.6	37	50	1.3
Sandstone	ML	-	2.15	10	0.7	15	25.4	37	40	1.0
Serpentinite	S	0	2.74	166	6.0	28	76.8	39	50	5.7
Serpentinite	S	90	2.75	74	16.3	5	39.4	39	49	5.6
Masterflow replica	R	-	2.10	47	5.4	9	16.4	13	-	-

gate the influence of different mechanical parameters on the shear strength and the failure mechanism. The mechanical properties of each rock type and replicas are reported in Table 4. Mechanical properties of rocks used in shear tests.. Forty-five shear tests have been conducted on fresh tensile rock joints using a servo-hydraulic shear apparatus, where jointed specimens are fixed into the upper and lower shear boxes and simultaneously subjected to normal and shearing stresses. Dilatancy, shear displacement and rotations are accurately measured and recorded using a PC equipped with a data-acquisition system. Before and after each constant normal load (CNL) shear test, the morphology of the joint is measured on a grid of 0.3 mm by 0.3 mm.

8. Cycles of shear tests on the same sample

In order to study the response of a joint to cyclic loads, several series of multiple shear tests have been conducted both on rock and replica samples.

It has been remarked that the friction value measured after 3 mm shearing during the first cycle (called ultimate friction) is constant, but is higher than the values obtained on the following cycles, which tend all to the same residual value (called residual friction; Figure 7).

This difference can be explained by the shearing of micro-roughness on contact areas. During the second shearing, as the shear-test starts again from the same position, most of the contact areas have already been smoothed. Therefore, the difference between the ultimate strength of a joint and the residual resistance could be used to quantify the influence of the micro-roughness on the joint friction. Even if only a few shear tests have been conducted, in the framework of this research, with horizontal displacement larger than five millimetres, the results show a constant, small decrease of the friction value to the residual strength. Thus, it is possible to argue that the ultimate friction will also decrease to the residual strength for large displacements during the first cycle.

It is evident that, by shearing the same fresh mated joints several times, only the first and eventually the second test present a resistance peak (Figure 7). For the other cases it is possible to identify only a yield point and a residual value for the shear strength.

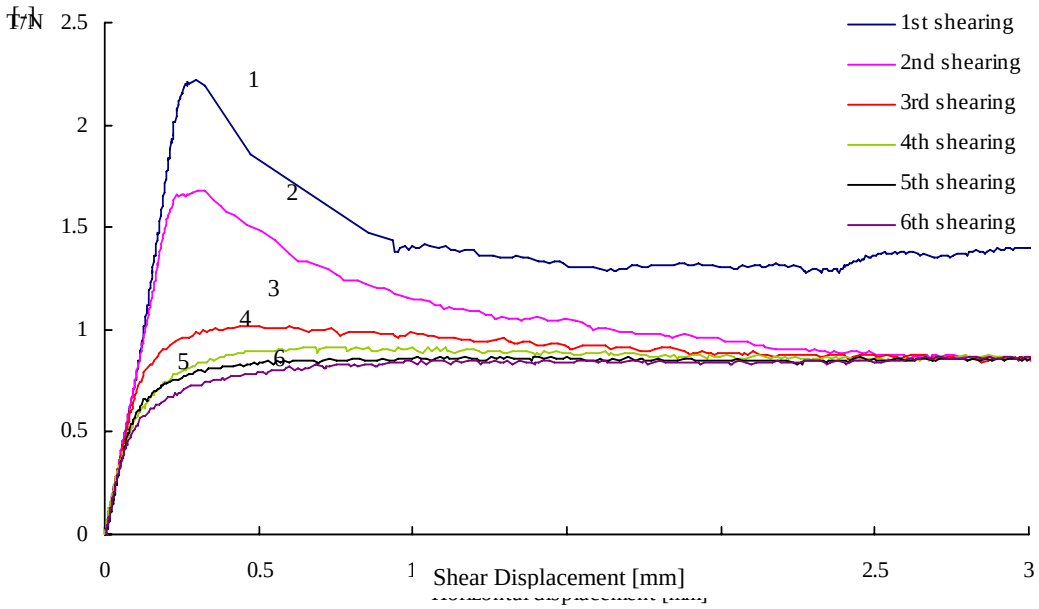

Sample	A_0	C	θ^*_{max}	l_x	l_y	α	u_p	N	σ_n/σ_c	T_p	T/N	ϕ_p	ϕ_r	$k_{s\ 50\%}$
S2	[-]	[-]	[deg]	[mm]	[mm]	[deg]	[mm]	[kN]	[-]	[kN]	[-]	[deg]	[deg]	[mm^{-1}]
1st cycle	0.466	4.44	75	140	140	0	0.4	38	1.2%	83	2.2	66	53	9.9
2nd cycle	-	-	-	140	140	0	0.37	38	1.2%	63	1.7	59	40	12.6
3rd cycle	-	-	-	140	140	0	0.46	38	1.2%	39	1.0	46	41	7.1
4th cycle	-	-	-	140	140	0	0.49	38	1.2%	34	0.9	42	41	6.8
5th cycle	-	-	-	140	140	0	0.5	38	1.2%	32	0.8	41	41	7.7
6th cycle	-	-	-	140	140	0	0.53	38	1.2%	30	0.8	40	40	7.1

Figure 7. Multiple shearing on the same serpentinite sample (S2) under 2 MPa constant normal load. After 5 mm of shear displacement, the sample was repositioned at the origin and sheared again.

9. Failure modes and implications for peak shear strength

Observations of the surfaces of several sheared rock joints indicated that tensile failure, rather than compressive failure, plays a major role in the breaking of individual asperities. Looking at the sheared joints, the areas where failure occurred tend to be rough, and it was possible to observe intact fragments sheared from the surface (particularly evident on surfaces where shearing was interrupted after small shear displacements). This approach is consistent with experimental results published by other authors [43,47-51]. Thus, it appears that tensile strength may be a more important parameter than compressive strength in quantifying the peak shear resistance of matching rock joints. This conclusion was important in deriving a more general expression for peak shear strength that holds for both mortar replicas and rock joints.

10. Peak shear strength criterion

In deriving a general expression for peak shear strength, a primary assumption was that the general mechanical behaviour of rock joints can be assumed to be similar to that of mortar replicas. The experimentally derived curves of τ_p/σ_n versus σ_n/σ_c (Figure 6) show that peak-shear strength decreases from a maximum finite value to a constant residual value with increasing σ_n, and also indicate that the curves have a negative-exponential shape. The experimental results presented here show that the peak friction angle, expressed according to Coulomb's expression by the ratio of shear-to-normal load,

$$\frac{\tau_p}{\sigma_n} = \tan \phi_p \,, \qquad (2)$$

never exceeds about 65-80 degrees, depending on the morphology of the joint. This is consistent with results presented by other researchers [3]. Thus, an expression for peak-shear strength should approach a finite value as the applied normal load approaches zero.

A second consideration was the importance of using the tensile strength of the rock rather than compressive strength, and of considering the roughness of the joint.

Taking into account these considerations and the test results, which suggest the overall shape of the curve, the following expression for peak shear strength is proposed:

$$\tau_p = \sigma_n \tan \phi_r^* \left[1 + e^{-\left(\frac{\theta^*_{\max}}{B} \frac{\sigma_n}{A_0 \, C \, \sigma_t} \right)} \right], \qquad (3)$$

where:

τ_p is the peak shear strength of the joint,

σ_n is the applied average normal stress,

σ_t is the tensile strength of the intact material obtained from a standard Brazilian test,

ϕ_r^* is the residual friction angle (measured after a standard displacement of 5 mm),

A_0 is the maximum potential contact area for the specified shear direction,

$\theta^*_{\max}$ is the maximum apparent dip angle with respect to the shear direction,

C is the roughness parameter.

The parameter B is a dimensionless fitting parameter. Multiple least-squares regression using the data obtained for all 37 rock-joint samples was used to estimate the value of B, and a value of 9.0 was obtained.

Thus, for induced joints in the rock types and mortar replicas used during this investigation, the following expression for peak shear strength is proposed:

$$\tau_p = \sigma_n \tan \phi_r^* \left[1 + e^{-\left(\frac{\theta^*_{\max}}{9} \frac{\sigma_n}{A_0 \, C \, \sigma_t} \right)} \right]. \qquad (4)$$

The expression inside the square brackets in equation 4 approaches the limiting value of two as the argument in the exponential term goes to zero. The argument in this term approaches zero if either $\theta^*_{\max}$ or σ_n approach zero. However, in practice, $\theta^*_{\max}$ is confined to a range of approximately 20 to 90 degrees. With respect to σ_n, as described in detail above, the minimum value occurs when there is no applied normal load, in which case the normal stress is that resulting from the weight of the sample itself. In this situation, as σ_n approaches zero, it is possible to show that

$$\lim_{\sigma_n \to 0} \left(\frac{\tau_p}{\sigma_n} \right) = 2 \tan \phi_r^* = \tan \phi_p \;\rightarrow\; \phi_p = 65^\circ \sim 80^\circ . \qquad (5)$$

The predictions of peak shear strength made with equation 4 agree well with the experimental results obtained in laboratory tests. However, since the objective of this study is to develop a simple method for estimating joint shear strength, equation 4 is not entirely satisfactory, because it requires an estimate of the residual friction angle, ϕ_r^*, for each sample. Since analysis of the laboratory results lead to the hypothesis that ϕ_r^* is function of the basic friction angle of the material, of the surface roughness of the specific joint, and of the internal structure of the rock itself, e.g., schistosity, also has an important effect, the functional form for incorporating these parameters was determined by experimenting with different expressions and comparing the results to the experimental data. There is much scatter in the experimental data, so the following empirical relationship is at best a rough approximation:

$$\phi_r^* = \phi_b + \beta_r = \phi_b + \left(\frac{\theta^*_{\max}}{C} \right)^{1.18 \cos \alpha} . \qquad (6)$$

If the rock does not exhibit schistosity, α is assumed to be equal to zero. The parameter β_r represents the

contribution of the roughness to the residual friction angle, which, according to the shear test results, takes on values in the range between 15 and 24 degrees.

Thus, substituting the empirical expression for the residual friction angle into equation 4, the final expression for peak shear strength of rock joint is:

$$\tau_p = \sigma_n \tan\left[\phi_b + \left(\frac{\theta^*_{\max}}{C}\right)^{1.18\cos\alpha}\right]\left[1 + e^{-\left(\frac{\theta^*_{\max}\,\sigma_n}{9\,A_0\,C\,\sigma_t}\right)}\right]. \quad (7)$$

The predictions of peak shear strength made with equation 7 agree well with the experimental results obtained in laboratory tests (Figure 8), and the great contribution to shear strength provided by surface roughness. A rough joint can more than double its shear resistance compared to a smooth one. Moreover, the anisotropy of the joint regarding the shear strength depend directly from its surface anisotropy. The estimated ϕ_{peak} values are in general agreement with those obtained experimentally (

Table 3).

11. Constitutive model for mated rock joints

Observing the experimental plots of shear strength versus horizontal displacement, it was noted that often the beginning of the test was characterised by the fact that the joint was not totally mated. Therefore, a small displacement occurred before the joint was able to provide all its strength. Thus, the horizontal peak shear displacement can be expressed as the sum of two contributions:

$$u_p = u_m + \Delta u_p, \quad (8)$$

where u_m is the horizontal displacement necessary to mate the joint (when the joint is assumed "fresh", it principally depends on the experimental set-up); and Δu_p is the horizontal deformation of the joint before the peak. Subtracting this mating displacement from the total peak displacement, it was observed that, on 140 mm-long samples tested, Δu_p assumed values between 0.27 and 0.65 mm.

Observing the experimental curves, as the joint is mated, it is possible to affirm that the joint deforms almost linearly up to the peak shear stress.

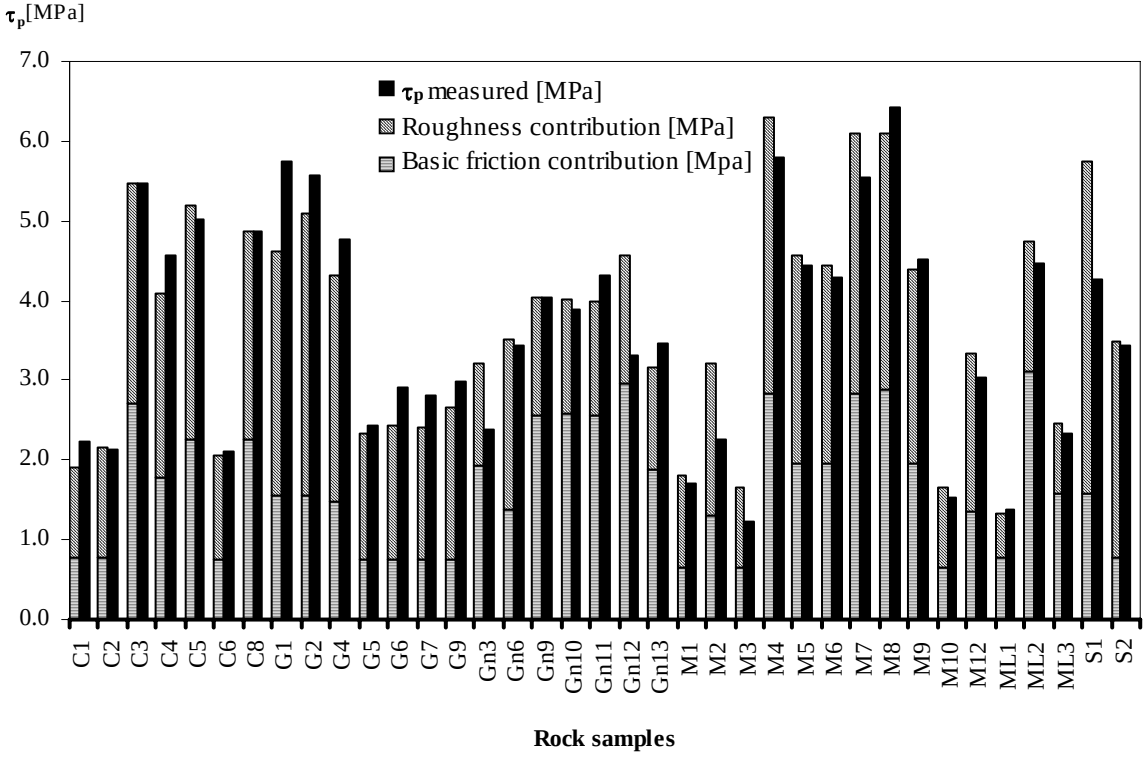

Figure 8. Contribution of the roughness to the estimation of the shear strength of the sample.

Therefore, a linear relation is used to describe the shear stiffness, k_s:

$$k_s = \frac{1}{\Delta u_p} \cdot \frac{\tau_p}{\sigma_n}, \tag{9}$$

where τ_p is the peak shear strength of the joint, σ_n is the applied average normal stress, and Δu_p is the horizontal deformation of the mated joint before the peak.

A negative slope of the stress-strain curve characterises the post-peak behaviour, where the shear strength of a joint falls to a constant value that corresponds to the ultimate/residual friction resistance of the joint. These considerations lead to the formulation of a model able to summarise the shear strength provided by the joint, under constant normal load conditions, at each state of displacement:

$$\begin{aligned} &\frac{\tau}{\sigma_n} = 0 && 0 \le u \le u_m \\ &\frac{\tau}{\sigma_n} = k_s \left(u - u_m\right) = \frac{1}{\Delta u_p} \frac{\tau_p}{\sigma_n} \left(u - u_m\right) && u_m \le u \le u_p \\ &\frac{\tau}{\sigma_n} = \frac{\tau_r}{\sigma_n} + \frac{\tau_p - \tau_r}{\sigma_n} \frac{u_p}{u} && u > u_p \end{aligned} \tag{10}$$

This expression shows that τ approaches the residual strength for values of displacement larger than u_r. The agreement between the constitutive model and the experimental results obtained in the laboratory is good (Figure 9).

12. Objective quantification of JRC

Each researcher who attempts to study the contribution of morphology to the shear strength has to deal with the JRC criterion proposed by Barton in the 1970s [3], and adopted as a reference by the International Society of Rock Mechanics in 1978 [7]. Therefore, considering that the peak shear strength value is unique for a given ex periment, for "fresh" joints ($JCS = \sigma_c$), it is possible t o equate equations 4 and Barton's one to obtain

$$JRC = \frac{\arctan\left\{\tan\left[\phi_b + \left(\theta^*_{\max}/C\right)^{1.18\,\cos\alpha}\right]\left[1 + e^{-\left(\frac{\theta^*_{\max}}{9}\frac{\sigma_n}{A_0}\frac{}{C}\frac{\sigma_n}{\sigma_t}\right)}\right]\right\} - \phi_b}{\log_{10}\left(\sigma_c/\sigma_n\right)} \tag{11}$$

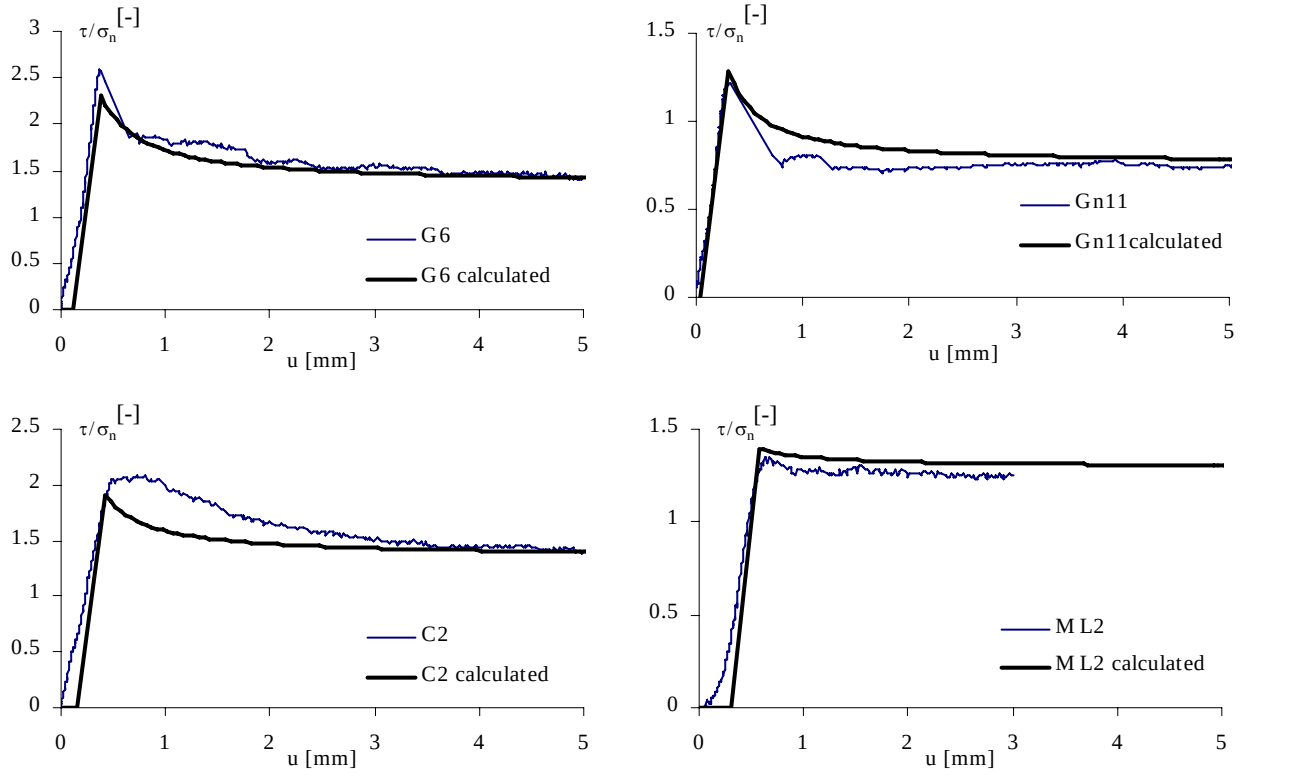

Figure 9. Comparison between laboratory experiments results and proposed constitutive model (Equation 10).

The JRC values calculated with back analysis of the experimental tests and those obtained with equation 11 are generally in rough agreement. The novelty of this approach to quantify JRC is that the three-dimensionality of the surface is considered, and the analysis is hence not reduced merely to a single profile.

13. Conclusions

The most important aspect of this research is the introduction of quantitative three-dimensional surface parameters into a peak shear strength criterion. The contribution of the roughness to the shear strength of the joint is, indeed, captured by parameters that are calculated on the entire joint surface, and not only on single profiles. The genesis of these parameters has the advantage of considering the directional micro-mechanical response of the entire sheared joint. Moreover, the residual shear strength of the joint is evaluated as a function of surface morphology and basic friction angle. The values of shear strength are reached rapidly after peak. Experimentally it was found that 5 mm after the peak, the joint strength has already reached its residual state.

It was shown that the proposed constitutive model is able to describe experimental shear tests for both replicas and fresh rock joints. Moreover, the parameters required to apply the model can be easily obtained through standard laboratory tests. From the literature, it appears that CNL and constant normal stiffness (CNS) tests have the same behavior up to peak shear stress; therefore, this approach may be valid for both boundary conditions up to peak stress. The proposed model was also used to calculate values of the joint roughness coefficient (JRC), resulting in a value that incorporates characteristics of the entire surface, rather than those of only a single arbitrary profile.

Nevertheless, in the current research, no attempt was made to investigate the influence of scale on the shearing. The results have validity only in the range of the samples tested in laboratory (σ_n/σ_c = 0.01 ~ 0.4 and σ_c/σ_t = 5 ~ 46).

A new approach is presented here for considering the influence of the rough joints in engineering problems, and it opens several avenues for both laboratory and field research. Indeed, rapidly changing technology is opening the door to not only high-resolution surface characterization in the laboratory, but also to new approaches that may allow joints to be characterized *in-situ*.

14. References

[1] Patton FD, Multiple modes of shear failure in rock. In Proc. 1st Congress of International Society of Rock Mechanics. Lisbon, Portugal, 1966, pp. 509-13.

[2] Ladanyi B, Archambault G, Simulation of the shear behaviour of a jointed rock mass. In Proc. 11th U.S. Symposium on Rock Mechanics. Berkeley, 1970, pp. 105-25.

[3] Barton N, Choubey V, The shear strength of rock joints in theory and practice. Rock Mech, 1977, **10**, 1-54.

[4] Amadei B, Wibowo J, Sture S, Price RH, Applicability of existing models to predict the behavior of replicas of natural fractures of welded tuff under different boundary conditions. Geotech Geo Eng, 1998, **16**, 79-128.

[5] Saeb S, Amadei B, Modelling rock joints under shear and normal loading. Int J Rock Mech Min Sci, 1992, **29**, 267-78.

[6] Plesha ME, Constitutive models for rock discontinuities with dilatancy and surface degradation. Int J Numer Anal Meth Geomech, 1987, **11**, 345-62.

[7] ISRM, Suggested methods for the quantitative description of discontinuities in rock masses. Int J Rock Mech Min Sci Geomech Abstr, 1978, **15**, 319-68.

[8] Den Outer A, Kaashoek JF, Hack HRGK, Difficulties with using continuous fractal theory for discontinuity surfaces. Int J Rock Mech Min Sci Geomech Abstr, 1995, **32**, 3-9.

[9] Huang SL, Oelfke SM, Speck RC, Applicability of fractal characterization and modelling to rock joint profiles. Int J Rock Mech Min Sci Geomech Abstr, 1992, **29**, 89-98.

[10] Lee YH, Carr JR, Barr DJ, Haas CJ, The fractal dimension as a measure of the roughness of rock discontinuity profiles. Int J Rock Mech Min Sci Geomech Abstr, 1990, **27**, 453-64.

[11] Muralha J, Fractal dimension of joint roughness surfaces. In Proc. Fractured and Jointed Rock Masses. Rotterdam, 1995, pp. 205-12.

[12] Xie H, Wang JA, Kwasniewski MA, Multifractal characterization of rock fracture surfaces. Int J Rock Mech Min Sci Geomech Abstr, 1999, **36**, 19-27.

[13] Odling NE, Natural fracture profiles, fractal dimension and joint roughness coefficients. Rock Mech Rock Eng, 1994, **27**, 135-53.

[14] Reeves MJ, Rock surface roughness and frictional strength. Int J Rock Mech Min Sci Geomech Abstr, 1985, **22**, 429-42.

[15] Tse R, Cruden DM, Estimating joint roughness coefficients. Int J Rock Mech Min Sci Geomech Abstr, 1979, **16**, 303-7.

[16] Maerz NH, Franklin JA, Bennett CP, Joint roughness measurement using shadow profilometry. Int J Rock Mech Min Sci Geomech Abstr, 1990, **27**, 329-43.

[17] Ferrero M, Iabichino G, Pancotti G, Giani GP, Interpretazione con modelli matematici di misure di rugosità di discontinuità naturali in roccia. In Proc. XX convegno nazionale di geotecnica. Parma, 1999, pp. 101-6.

[18] Hsiung SM, Ghosh A, Ahola MP, Chowdhury AH, Assessment of conventional methodologies for joint roughness coefficient determination. Int J Rock Mech Min Sci Geomech Abstr, 1993, **30**, 825-9.

[19] Aydan Ö, Shimizu Y, Kawamoto T, The anisotropy of surface morphology characteristics of rock discontinuities. Rock Mech Rock Eng, 1996, **29**, 47-59.

[20] Jing L, Nordlund E, Stephansson O, An experimental study on the anisotropy and stress-dependency of the strength and deformability of rock joints. Int J Rock Mech Min Sci Geomech Abstr, 1992, **29**, 535-42.

[21] Kulatilake PHSW, Shou G, Huang TH, Morgan RM, New peak shear strength criteria for anisotropic rock joints. Int J Rock Mech Min Sci Geomech Abstr, 1995, **32**, 673-97.

[22] Lee JJ, Bruhn RL, Structural anisotropy of normal fault surfaces. J Struct Geol, 1996, **18**, 1043-59.

[23] Riss J, Gentier S, Archambault G, Flamand R, Sheared rock joints: dependence of damage zones on morphological anisotropy. Int J Rock Mech Min Sci, 1997, **34**, 537.

[24] Lanaro F, Jing L, Stephansson O, 3-D-laser measurements and representation of roughness of rock fractures. In Proc. Mech Jointed Faulted Rock. Vienna, 1998, pp. 185-9.

[25] Belem T, Homand-Etienne F, Souley M, Quantitative Parameters for Rock Joint Surface Roughness. Rock Mech Rock Eng, 2000, **33**, 217-42.

[26] Grasselli G, Egger P, 3D surface characterization for the prediction of the shear strength of rough joint. In Proc. Eurock 2000. Aachen, Germany, 2000, pp. 281-6.

[27] Gentier SS, Hopkins DL, Mapping fracture aperture as a function of normal stress using a combination of casting, image analysis and modelling techniques. Int J Rock Mech Min Sci Geomech Abstr, 1997, **34**, 359.

[28] Re F, Scavia C, Determination of contact areas in rock joint by X-ray computer tomography. Int J Rock Mech Min Sci Geomech Abstr, 1999, **36**, 883-90.

[29] Nakagawa S, Hopkins D, Gentier S, Riss J, Hydromechanical behavior of fractures in shear: implications for seismic imaging. In Proc. ISRM9. Paris, 1999, pp. 947-51.

[30] Dong WP, Sullivan PJ, Stout KJ, The significance of surface features in characterising 2-D and 3-D surface topography. In Engineered Surfaces. Edited by Ehmann KF, Wilson WRD, Asme, 1993, pp 1.

[31] Myshkin NK, Petrokovets MI, Chizhik SA, Simulation of real contact in tribology. Tribology Int, 1998, **31**, 79-86.

[32] Bergmann D, Galanulis K, Winter D, Advanced 3D fringe projection system. 1997. http://www.gom.com/pub/publications/fringe-en.pdf

[33] Wirth J, Rapid Modeling. Munich, Hanser, 2002. ISBN 3-446-21380-5.

[34] Gentier S, Riss J, Archambault G, Flamand R, Hopkins DL, Influence of fracture geometry on sheared behavior. Int J Rock Mech Min Sci Geomech Abstr, 2000, **37**, 161-74.

[35] Kimura T, Esaki T, A new model for the shear strength of rock joints with irregular surfaces. In Proc. Mech Jointed Faulted Rock. Vienna, 1995, pp. 133-8.

[36] Yang ZY, Chiang DY, An experimental study on the progressive shear behavior of rock joints with tooth-shaped asperities. Int J Rock Mech Min Sci Geomech Abstr, 2000, **37**, 1247-59.

[37] Haberfield CM, Johnston IW, A mechanistically-based model for rough rock joint. Int J Rock Mech Min Sci Geomech Abstr, 1994, **31**, 279-92.

[38] Yeo IW, de Freitas MH, Zimmerman RW, Effect of shear displacement on the aperture and permeability of a rock fracture. Int J Rock Mech Min Sci, 1998, **35**, 1051-70.

[39] Gentier S, Lamontagne E, Archambault G, Riss J, Anisotropy of flow in a fracture undergoing shear and its relationship to the direction of shearing and injection pressure. Int J Rock Mech Min Sci, 1997, **34**, 412.

[40] Grasselli G, Wirth J, Egger P, Quantitative three-dimensional description of a rough surface and parameter evolution with shearing. Int J Rock Mech Min Sci, 2002, **39**, 789-800.

[41] Grasselli G, Wirth J, Zimmerman RW, Functional parameters for quantifying the surface anisotropy of rock discontinuities. In Proc. Eurock2002. Funchal (Madeira Island), Portugal, 2002, pp. 727-33.

[42] Flamand R, Validation d'une loi de comportement mécanique pour les fractures rocheuses en cisaillement. Ph.D. thesis, University of Quebec, Chicoutimi, 2000.

[43] Huang TH, Chang CS, Chao CY, Experimental and mathematical modeling for fracture of rock joint with regular asperities. Eng Fract Mech, 2002, **69**, 1977-96.

[44] Ohnishi Y, Dharmaratne PGR, Shear behaviour of physical models of rock joints under constant normal stiffness condition. In Proc. Rock Joints. Loen, Norway, 1990, pp. 267-73.

[45] Skinas CA, Bandis SC, Demiris CA, Experimental investigations and modelling of rock joint behaviour under constant stiffness. In Proc. Rock Joints. Loen, Norway, 1990, pp. 301-8.

[46] Olsson R, Barton N, An improved model for hydromechanical coupling during shearing of rock joints. Int J Rock Mech Min Sci, 2001, **38**, 317-29.

[47] Fishman YA, Failure mechanism and shear strength of joint wall asperities. In Proc. Rock Joints. Loen, Norway, 1990, pp. 627-31.

[48] Handanyan JM, Danek ER, Dandrea RA, Sage JD, The role of tension in failure of jointed rock. In Proc. Rock Joints. Loen, Norway, 1990, pp. 195-202.

[49] Kutter HK, Otto F, Influence of parallel and cross joints on shear behaviour of rock discontinuities. In Proc. Rock Joints. Loen, Norway, 1990, pp. 243-50.

[50] Pereira JP, De Freitas MH, Mechanism of shear failure in artificial fractures of sandstone and their implication for models of hydromechanical coupling. Rock Mech Rock Eng, 1993, **10**, 1-54.

[51] Armand G, Contribution à la caractérisation en laboratoire et à la modélisation constitutive du comportement mécanique des joints rocheux. Ph.D. thesis thesis, Universite Joseph Fourier, Grenoble, France, 2000.